OPEN

Synthesis of Au/SnO$_2$ nanostructures allowing process variable control

Myung Sik Choi[1,6], Han Gil Na[1,6], Sangwoo Kim[2,6], Jae Hoon Bang[1], Wansik Oum[1], Sun-Woo Choi[3], Sang Sub Kim[4], Kyu Hyoung Lee[5], Hyoun Woo Kim[1*] & Changhyun Jin [5*]

Theoretical advances in science are inherently time-consuming to realise in engineering, since their practical application is hindered by the inability to follow the theoretical essence. Herein, we propose a new method to freely control the time, cost, and process variables in the fabrication of a hybrid featuring Au nanoparticles on a pre-formed SnO$_2$ nanostructure. The above advantages, which were divided into six categories, are proven to be superior to those achieved elsewhere, and the obtained results are found to be applicable to the synthesis and functionalisation of other nanostructures. Furthermore, the reduction of the time-gap between science and engineering is expected to promote the practical applications of numerous scientific theories.

Currently, although the boundaries of the academic area do not seem to be important, a clear-cut borderline separates pure science[1,2], which explores the principles of nature, from applied engineering[3,4], which deals with real-life processes. This separation largely reflects the corresponding difference in the utilised approaches, high-lighting the fact that the application of new theories to real-world problems is difficult and time-consuming. For this reason, scientific heritage newly published every day is often discarded without actually being phenomeno-logically expressed. On the contrary, our daily life presents numerous strange phenomena that cannot be scien-tifically explained because of the lack of a proper academic background. That is, there may be cases of a theory not backed by experimental results or results not explained by any theory. As mentioned above, science and engineering can be viewed to be in a state of temporal hysteresis, and the search for ways of narrowing the cor-responding time gap should therefore be regarded as a task of high significance. For example, Shi *et al.* reported the hetero-structured AgBr/ZnO photocatalyst, but their synthesis requires long reaction times and complex multi-step processes[5]. Ellis *et al.* also proposed the morphology control of hydrothermally prepared LiFePO4 with long reaction times and post heat treatment processes[6]. In other words, engineering techniques that can easily and economically confirm competitive scientific theories are shortcuts that can reduce the time cost of the practical application of science and achieve unique and meaningful results. Unluckily, because of the atmos-phere that emphasises originality in research, one tends to think that only complicated and difficult-to-perform experiments can produce unique results. However, the reason why we cannot conclude that it is preconceived is that many of the results have received good evaluation in the meantime. For example, when studies on various nanostructures[7–10] performed so far are divided into those dealing with morphology[11,12], crystallography[13,14], and elemental composition[15,16] control, one can recognise that these investigations have a certain research value when the desired shape, microstructure, or function has been fully achieved. In this case, the employed raw materials and equipment are costly, the use of in-house-made equipment precludes verification in other laboratories, the experiment condition that was different from the existing experiment was exactly met in the repeated experiment, and technological differences related to the use of high-end analytical equipment are rarely considered. In other words, the outcomes of such experiments emphasise specificity rather than generality, and consequently require much time to be verified by engineering in real life, i.e., in such cases, one can only imply that a new theory can

[1]Division of Materials Science and Engineering, Hanyang University, Seoul, 04763, Republic of Korea. [2]Liquid Processing and Casting R&D Group, Korea Institute of Industrial Technology, 156, Getpearl-ro, Yeonsu-gu, Incheon, 21999, Republic of Korea. [3]Department of Materials Science and Engineering, Kangwon National University, Samcheok, 25913, Republic of Korea. [4]Department of Materials Science and Engineering, Inha University, Incheon, 402-751, Republic of Korea. [5]Department of Materials Science and Engineering, Yonsei University, Seoul, 03722, Republic of Korea. [6]These authors contributed equally: Myung Sik Choi, Han Gil Na and Sangwoo Kim. *email: hyounwoo@hanyang.ac.kr; chjin0910@gmail.com
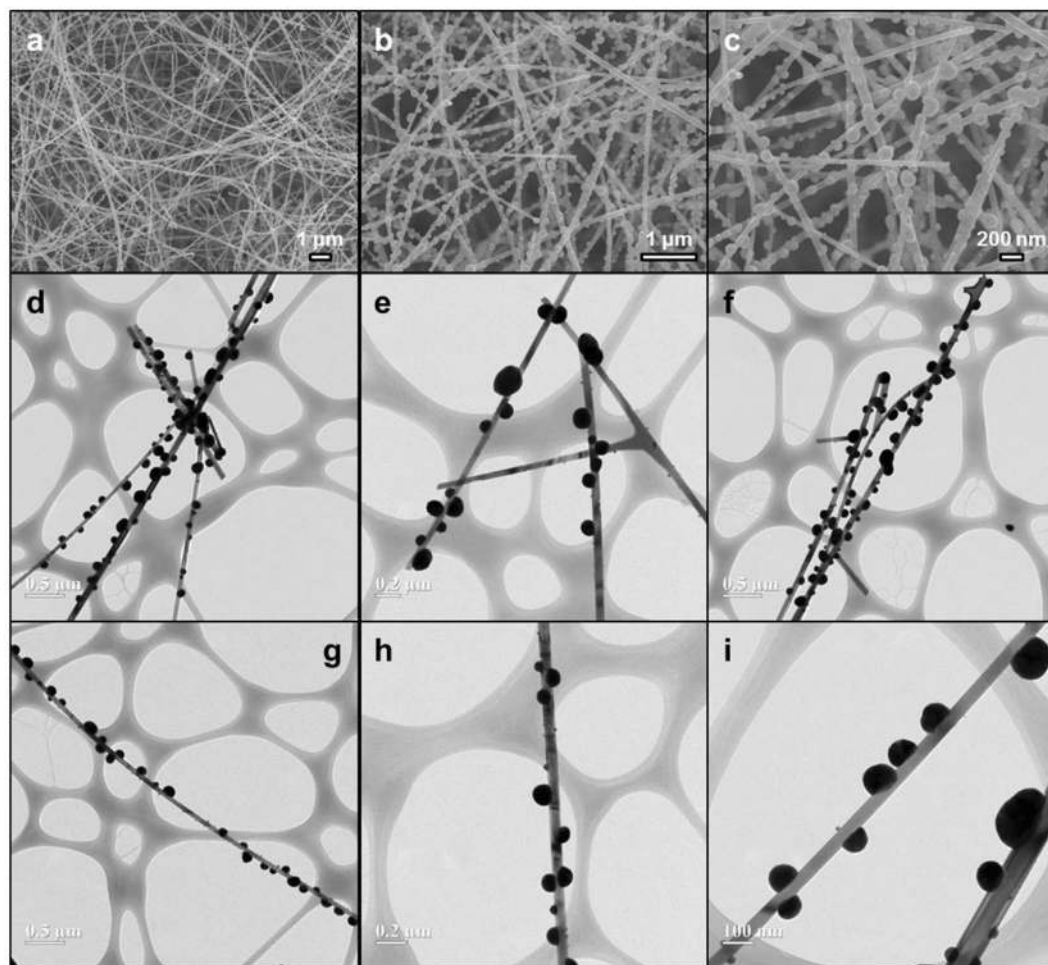
Figure 1. Typical SEM and TEM images of SnO$_2$ nanowires formed by conventional thermal evaporation and of Au particles formed on SnO$_2$ nanowires by flame chemical vapour deposition. (**a**) SEM image of bare SnO$_2$ nanowires with a smooth surface; (**b**) low-magnification and (**c**) high-magnification SEM images of Au-SnO$_2$ hybrid nanostructures; (**d–i**) variable-magnification TEM images of Au-SnO$_2$ nanostructures of different shapes.

be realised. Herein, we introduce new processing advantages to easily fabricate a heterogeneous structure by attaching Au particles to pre-formed SnO$_2$ nanostructures and compare the advantages of our work with the disadvantages of existing works in six representative categories used in science/engineering fields. The proposed method allows one to induce nucleation and growth in nanostructures in a shorter time than in the case of other synthesis/deposition techniques. Moreover, thermal energy injection allows the phase change and composition to be relatively easily altered, and the developed technique also allows one to easily change the shape and micro-structure of pre-formed nanostructures, which is attributed to energy injection variation with temperature and holding time. Thus, in contrast to the existing principle of one-to-one matching, which assumes that one factor depends on one process variable, the described technique utilises a new one-to-many matching concept, allowing one to simultaneously control multiple factors with one process variable.

Result and Discussion

Figure 1 shows Au particle–decorated SnO$_2$ nanostructures prepared under various experimental conditions. As is well known[17,18], smooth and long SnO$_2$ nanowires can be easily synthesised by thermal evaporation of Sn powder in an oxygen-containing atmosphere. Herein, the thickness of SnO$_2$ nanowires ranged from 20 to 120 nm, and their length ranged from several tens to several hundred μm (Fig. 1a–c). However, when a 5-s energy pulse was applied to SnO$_2$ nanowires that had previously been exposed to HAuCl$_4$·4H$_2$O/(CH$_3$)$_2$CHOH, the originally smooth surface of SnO$_2$ nanowires got covered by Au particles and therefore became rough. The spherical Au particles attached to nanowires had a size of roughly 100–300 nm and were in a discrete state (Fig. 1d–i). Specifically, these particles did not aggregate to lower their surface energies and existed independently at regular intervals, which was ascribed to the fact that the thermal energy applied to SnO$_2$ nanowires was not concentrated in a narrow region adjacent to nanowires but was uniformly dispersed in space. In other words, it was concluded that the applied thermal energy allowed the rate of nucleation to be held constant at all points of SnO$_2$ nanowires. Thus, it could be said that this simultaneous energy injection was different from the general mechanism of nucleation and growth in the local region of interest. Only morphologically, Au-decorated SnO$_2$ nanostructures

can be prepared in any number of ways. However, most of these methods refrain from instantaneous processing to increase the cross-sectional area and require various pre- and post-processing techniques[19–21]. For example, Kim *et al.* synthesised noble metal–decorated SnO_2 nanowires using thermal activation and employed the large cross-sectional area of these nanoparticles to detect noxious gases[22]. Wu *et al.* suggested that hydrothermally prepared hollow hybrid Au-SnO_2 nanostructures can be utilised in photocatalysis application[23], with advantages such as environmentally friendly solution-basis, low-cost, and surfactant-free. Bing *et al.* used a rational combinational multi-step synthetic route to prepare Au-loaded SnO_2 hollow multi-layered nanosheets, composed of numerous nanoparticles as structural subunits[24]. Furthermore, although previous reports could realise nanocomposite structures of the abovementioned morphology[25,26], they remain inferior in terms of speed, accuracy, yield, and economy, i.e., accessibility. For example, Lai *et al.* realised heterogeneous nucleation sites using a template with a low vaporisation point and fabricated nanobeads by subsequent template removal at high temperatures[27]. Some studies suggested that Pd-functionalised nanostructures can be formed by post-heat treatment and/or electron beam irradiation, without the involvement of extra precursors, because extra energy itself facilitates nucleation at an energy lower than that of homogeneous nucleation[28,29]. However, in the two cases mentioned above, there is no way to control nanowire parameters until the end stage, since metal particle nuclei are formed on the metal oxide before or during synthesis. That is, if the desired metal-decorated nanowires are not obtained, the experiment needs to be re-started from the very beginning. In contrast, our method relies on simultaneous annealing, allowing one to rapidly functionalise existing SnO_2 nanowires in the desired way. This advantage cannot be found in any other post-processing technique, and one can therefore say that in addition to the abovementioned five advantages (speed, accuracy, yield, economy, and accessibility), our method also guarantees stability.

As shown in Fig. 1d–i, even though rugged Au particles were commonly observed on the originally smooth SnO_2 nanowires, bigger Au spheres were sometimes formed on the surface of certain SnO_2 nanowires through interfacially controlled spherical growth[30]. The above figures indicate no change in the morphology of Au-decorated nanowires; however, even in a localised region, the size of Au particles produced on nanowires tended to decrease with increasing time of thermal energy injection in that region. This behaviour was ascribed to the role of injected heat energy in inducing simultaneous nucleation over a large area, so that the effect of growing the nucleated first in a momentary difference is relatively insufficient. Therefore, as the retention time of energy injection at each point increased, the distance between Au particles generated in the nanowire decreased, while the density of Au particles produced at a fixed length increased. These results are in stark contrast with the fact that after nucleation, the rapid growth of nanostructures is commonly controlled by the rate of constituent atom diffusion[31].

The above finding indicates that the increase of supplied energy amount with increasing heating time is related to the reduction of SnO_2 accompanied by the formation of Au (Fig. 2). Thus, even for Au-decorated SnO_2 of the same type, the reduction gradient is determined by the energy injection time (heating time). To investigate the degree of reduction, all samples were subjected to elemental mapping (Fig. 2a–d) and EDX (Fig. 2e–h) measurements, which revealed that the Sn:O ratio was different in nanowires and Au particles, as described above. In SnO_2 nanowires, Au was not observed at all (Fig. 2e,f), but Sn and O were detected together with Au in the particle region (Fig. 2g,h). That is, the precipitation of Au and the reduction of SnO_2 occurred simultaneously. This behaviour probably reflects the fact that when the Au solution was pushed to one side to become a particle as a result of energy supply, a part of the SnO_2 nanowire surface was exposed and lost O because of the effect of direct energy injection. Thus, one has only started exploring the applications of these two effects, which are believed to have much scientific and engineering potential.

For each sample, the crystal phase composition and microstructure were verified by XRD (Fig. 3a) and TEM (Fig. 3b–g), respectively. Bare SnO_2 nanowires were shown to have a tetragonal structure[32], and peaks at $2\theta = 26.61°$, 33.89°, 37.95°, 38.97°, and 42.63° were in good agreement with reflections from (110), (101), (200), (111), and (210) planes of tetragonal SnO_2, respectively (JCPDS No. 41–1445) (Fig. 3a)[33]. Peaks at $2\theta = 38.18°$ and 44.39° were ascribed to reflections from the (111) and (200) planes of Au (JCPDS No. 04–0784), respectively[34] (Fig. 3a). On the other hand, for samples prepared by applying thermal energy to bare SnO_2 nanowires, we observed a change of SnO_2 peak intensity and the appearance of new peaks. As described above, a reduction of SnO_2 to Sn may occur under the employed conditions, which may result in the formation of non-equilibrium SnO_x $(0 < x < 2)$ phases (Fig. 3b–g). Although these peaks did not exactly match those in JCPDS cards because of the non-equilibrium nature of the former, such chemical changes could be sufficiently inferred from the shift of the (101) peak of pre-formed SnO_2 to the (101) peak of Sn. At this time, a SnO_2 layer was detected on the surface of SnO_2 nanowires (Fig. 3d,f) and on the surface of Au particles (Fig. 3e). However, interplanar spacings of unbalanced compositions could be observed with proceeding partial reduction. In other words, no crystal phases except for those of SnO_2 and Au were observed by XRD, although HRTEM line profiling indicated that the surface profiles of SnO_2 or Au could change. This means that the energy supplied to the existing SnO_2 nanowires was sufficient for SnO_x to form on the Au surface (Fig. 3d–g).

The efficiency of making Au-SnO_2 should be further objectified to allow the clear application of the competitiveness of the new method and its difference from the existing techniques. Consequently, the process methods were evaluated using six parameters (Tables 1, 2, S1 and S2), namely the employed precursor, equipment, pre- and post-treatment, temperature, time, and vacuum[35–66]. First, the new processing technique was found to be applicable to all materials regardless of their type. Second, while the previously used equipment occupies much space, requiring additional equipment to achieve the special purpose, our processing technology is not affected by location and does not involve the utilisation of useless accessories. Third, researches conducted so far, especially those requiring pre-processing such as templating and post-processing such as heat treatment, have often involved supplementary procedures to address the difficulty of direct synthesis and deposition, whereas our high-efficiency method does not require any pre- or post-processing. Fourth, in previous methods, the temperature had to be maintained within the range of at least 500 to 1000 °C for a long time to adjust the synthesis temperature of
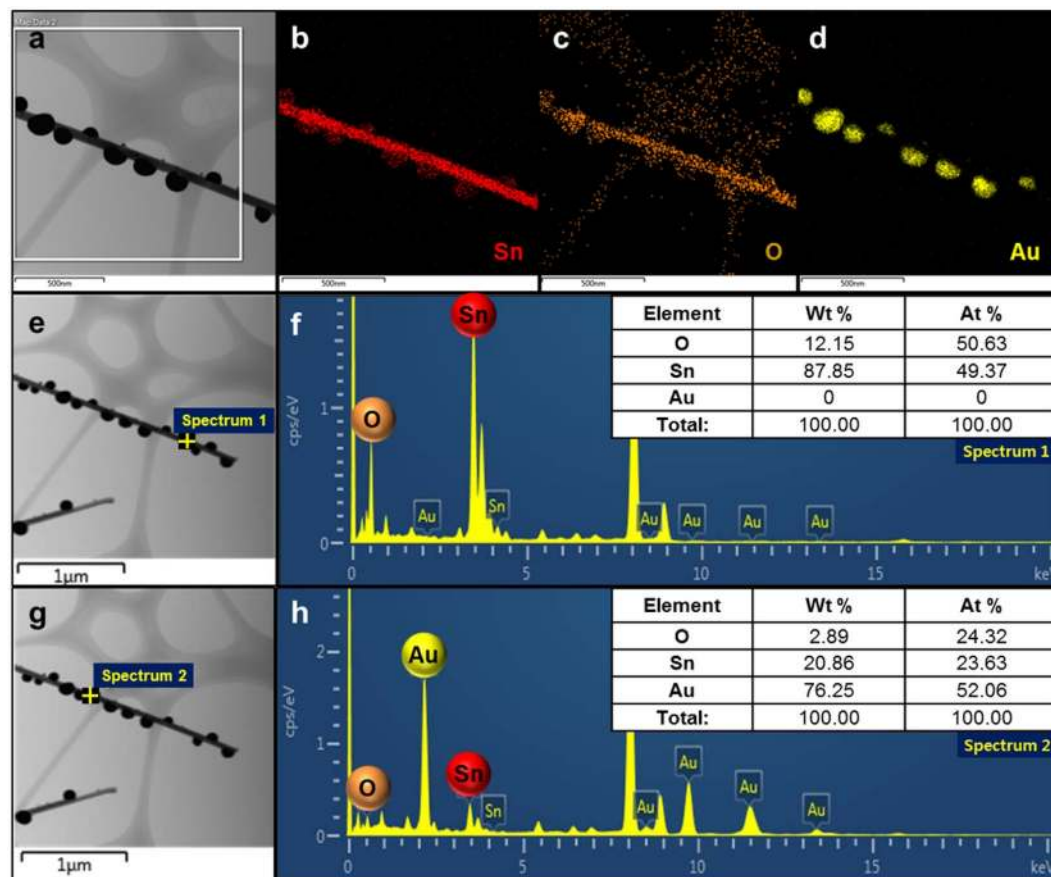
Figure 2. Zone composition of Au-SnO$_2$ hybrid nanostructures identified by elemental mapping and EDX. (**a**–**d**) Distributions of Sn, O, and Au in a typical Au-decorated SnO$_2$ nanowire; (**e,f**) contents of Sn and O in a SnO$_2$ nanowire determined excluding Au particles; (**g,h**) contents of Sn, O, and Au in a Au particle excluding the SnO$_2$ nanowire.

heterogeneous materials, whereas our method instantaneously provides a temperature of 1300 °C. Fifth, our process is operated on a timescale of seconds and is clearly different from other processes operated on the time scales of minutes or even hours, allowing one to control instantaneous processing conditions on the spot to match material properties. Sixth, conventional synthesis and deposition equipment requires the use of variable (low to ultra-high) vacuum depending on the specific case, whereas our technique does not require additional vacuum conditions, since it can be operated under atmospheric pressure. There may be many other classification criteria, but it seems clear that the above six advantages provide overwhelming evidence of the superiority of our method.

As mentioned above, differences between science and engineering inevitably result in the need for a certain time period to achieve coincidence. In most cases, a theory is first established, and the corresponding time-saving potential is evaluated in the next step. Therefore, it is meaningful to find a new method allowing one to control several variables through a simple experiment, which can simplify the whole process but produce various results. In the meantime, we have invested a lot of time and money in the synthesis and functionalisation of new materials with novel properties. Thus, the know-how to produce the desired results with this simple method can be applied to other materials in the same way, and the search for even simpler and more powerful derivation methods should not be stopped.

Conclusion

A new method of synthesising SnO$_2$ and converting it to a different standard has been proposed. This method allows one to relatively easily control the parameters of Au-decorated SnO$_2$ nanowires using thermal energy, i.e., the growth factors for each sample can be freely controlled depending on the given materials and processing time. Specifically, the reaction proceeds from a homogeneous structure to a heterogeneous structure, or from a stoichiometric structure to a non-stoichiometric structure, depending on the amount of applied energy. The trend of this transition is also consistent with the results of SEM, XRD, and TEM analyses. This seemingly ordinary process technology has proven to be overwhelmingly superior in terms of precursor, equipment, pre- and post-treatment, temperature, time, and vacuum. From an energy point of view, all experimentation with science/engineering bases relies on the idea of making a difference in energy or eliminating the energy difference. Thus, the ability to achieve a variety of effects by reducing the number of process variables and simply adjusting them should substantially contribute to reducing the congenital time gap between science and engineering.

| This work | Other work | | | | |
	Composites	Precursor	Equipment	Pre- and post- treatment	Ref.
Composites: SnO_2 NWs - Au NPs	TiO_2 NTs-Ag NPs	$AgNO_3$, Salicylic acid	DC current power supply, stirrer, furnace	anodization, stirring	35
	WO_3 NFs-Rh_2O_3 NPs	Rhodium chloride hydrate, butanediol, PVP, sodium citrate, acetone, ammonium metatungstate hydrate	centrifugal separator, stirrer, furnace, DC voltage supply	centrifugation, stirring	36
	ZnO NWs-Cr_2O_3 NPs	$CrCl_2$	furnace	—	37
	SnO_2 NWs-Ag NPs	Ag filament	furnace	—	38
Precursor: Gold Chloride hydrate, 2-propanol	WO_3 NRs-Pd NPs	$PdCl_2$, ethanol	furnace	—	39
	SnO_2 NWs-Cr_2O_3 NCs	$CrCl_2$	furnace	—	40
	RuO_2 NRs-Ru NPs	—	furnace	thermal reduction	41
	TiO_2 NRs-NiO NPs	$NiCl_2 \cdot 6H_2O$, 2-methoxyethanol, ammonia	stirrer, furnace	stirring	42
	TiO_2 NWs-Au NPs	$HAuCl_4 \cdot 3H_2O$, NaOH	furnace	$AgNO_3$ test	43
	ZnO_2 NWs-TiO_2 NPs	TiO_2 suspension (P25), acetylacetone, Triton X-100, D.I water, ethanol, acetic acid	furnace, sonicator	sonication	44
Equipment: FCVD equipment	WO_3 NWs-PdO NPs	Palladium acetylacetonate, acetone	stirrer, sonicator, furnace	stirring, sonication, furnace	45
	WO_3 NWs-PtO_x NPs	Platinum acetylacetonate, acetone	stirrer, sonicator, furnace	stirring, sonication, furnace	45
	CuO NWs-Au NPs	Au target	sputter, furnace	sputtering	46
	SnO_2 NWs-Pd NPs	Au target, Sn powder, pluronic (P123) surfactant, $PdCl_2$, $NaCl_2$	sputter, furnace, stirrer	sputtering, stirring	47
Pre- and post- treatment: Nothing	TiO_2 NFs-Pt NPs	Ethylene glycol, PVP, H_2PtCl_6	furnace	—	48
	ZnO NWs-Au NPs	$HAuCl_4 \cdot 4H_2O$, ethanol	UV box, furnace	—	49
	ZnO NWs-Pd NPs	$PdCl_2$	furnace	—	50
	MoO_3 NWs-Ag NPs	$AgNO_3$	stirrer, vacuum oven	stirring, filtering, post-cleaning	51
	SnO_2 NFs-Pt NPs	H_2PtCl_6, ethylene glycol, PVP, acetone	centrifugal separator, furnace	centrifugation, post-cleaning	52
	ZnO NWs-Au NPs	$HAuCl_4$, Na_2CO_3	stirrer, furnace	stirring	53
	WO_3 NWs-Pd NPs	$PdCl_2$, D.I water, HF	furnace, sonicator	sonication	54
	WO_3 NWs-Pt NPs	Ethylene glycol, PVP, H_2PtCl_6, acetone, D.I water, ethanol	furnace, centrifugal separator	centrifugation, post-cleaing	55
	SnO_2 NWs-Cr_2O_3 NPs	Cr target	sputter, furnace	sputtering	56
	ZnO NWs-CdS NPs	$CdSO_4$, NH_4OH	furnace	—	57
	V_2O_5@ZnO-Au NPs	$HAuCl_4$, D.I water	furnace	—	58
	ZnO NW-Au NPs	Citrated-stabilized Au	—	—	59
	SnO_2 NFs-Pt NPs	H_2PtCl_6, ethylene glycol, PVP, acetone, D.I water	furnace, centrifugal separator	centrifugation, post-cleaning	60
	Zn_2SnO_4 NWs-ZnO QDs	Zinc acetate dihydrate, ethanol	autoclave	—	61
	GaN NWs-TiO_2 NCs	TiO_2 target	RF sputter, furnace	sputtering	62
	SnO_2 NWs-NiO NPs	NiO	furnace	thin film deposition	63
	SnO_2 NWs-CdS QDs	$CdSO_4$, thiourea, ammonia	oil bath, furnace	—	64
	ZnS NWs-CuO NPs	$CuSO_4$, NaOH, D.I water, acetone, isopropyl alcohol	furnace, sonicator, stirrer, centrifugal separator	sonication, stirring, centrifugation	65
	TiO_2 NWs-Ag NPs	D.I water, ethanol, NaOH, $AgNO_3$	sonicator, furnace	sonication	66

Table 1. Comparison of our process with previously reported ones.

This work	Other work				
	Composites	Temp.	Time required	Degree of vacuum	Ref.
	TiO$_2$ NTs-Ag NPs	500 °C 80 °C 80 °C 500 °C	2 hr (500 °C) 3 hr (80 °C) 1 hr (80 °C) 3 hr (500 °C)	—	[35]
Composites: SnO$_2$ NWs - Au NPs	WO$_3$ NFs-Rh$_2$O$_3$ NPs	686 °C 600 °C	20 min (686 °C) 1 hr (600 °C)	Air	[36]
	ZnO NWs-Cr$_2$O$_3$ NPs	630 °C	20 min	~9 × 10^{-2} torr	[37]
	SnO$_2$ NWs-Ag NPs	300 °C	1 hr	~10^{-6} torr	[38]
	WO$_3$ NRs-Pd NPs	500–700 °C	30 min (500–700 °C)	0.1 torr	[39]
	SnO$_2$ NWs-Cr$_2$O$_3$ NCs	620 °C	20 min	~9 × 10^{-2} torr	[40]
Temp.: 1300 °C	RuO$_2$ NRs-Ru NPs	650 °C 130 °C	20–120 min (650 °C) 1 hr (130 °C)	~4 × 10^{-5} torr (650 °C) 0.4–1.0 torr (130 °C)	[41]
	TiO$_2$ NRs-NiO NPs	40 °C 60 °C 600 °C	1 hr (40 °C) 10 min (60 °C) 1 hr (600 °C)	1 torr	[42]
	TiO$_2$ NWs-Au NPs	70 °C 100 °C 200 °C	2 hr (70 °C) 12 hr (100 °C) 4 hr (200 °C)	Air	[43]
	ZnO$_2$ NWs-TiO$_2$ NPs	450 °C	30 min	Air	[44]
Time required: 5 s	WO$_3$ NWs-PdO NPs	300 °C	2 hr	Air	[45]
	WO$_3$ NWs-PtO$_x$ NPs	300 °C	2 hr	Air	[45]
	CuO NWs-Au NPs	500 °C	30 min	Air	[46]
	SnO$_2$ NWs-Pd NPs	45 °C	12 hr	—	[47]
	TiO$_2$ NFs-Pt NPs	110 °C	30 min	—	[48]
	ZnO NWs-Au NPs	480 °C	1 hr	—	[49]
	ZnO NWs-Pd NPs	400 °C	4 hr	Air	[50]
Degree of vacuum: Air	MoO$_3$ NWs-Ag NPs	0 °C RT (25 °C) 80 °C	30 min (0 °C) 24 hr (RT) 2 hr (80 °C)	—	[51]
	SnO$_2$ NFs-Pt NPs	500 °C	2 hr	Air	[52]
	ZnO NWs-Au NPs	400 °C	4 hr	—	[53]
	WO$_3$ NWs-Pd NPs	100 °C 400 °C	4 min (100 °C) 1 hr (400 °C)	—	[54]
	WO$_3$ NWs-Pt NPs	150 °C	1 hr	—	[55]
	SnO$_2$ NWs-Cr$_2$O$_3$ NPs	700 °C	2 hr	Air	[56]
	ZnO NWs-CdS NPs	60 °C	40–250 min	—	[57]
	V$_2$O$_5$@ZnO-Au NPs	350 °C	1 hr	—	[58]
	ZnO NW-Au NPs	RT (25 °C)	12–18 hr	—	[59]
	SnO$_2$ NFs-Pt NPs	150 °C	2 hr	—	[60]
	Zn$_2$SnO$_4$ NWs-ZnO QDs	95 °C	2 hr	—	[61]
	GaN NWs-TiO$_2$ NCs	650–700 °C	30 s	—	[62]
	SnO$_2$ NWs-NiO NPs	400 °C	5 hr	—	[63]
	SnO$_2$ NWs-CdS QDs	60 °C 400 °C	30 min (60 °C) 2 hr (400 °C)	—	[64]
	ZnS NWs-CuO NPs	150 °C 500 °C	1 min (150 °C) 1 hr (500 °C)	1 mtorr	[65]
	TiO$_2$ NWs-Ag NPs	50–60 °C	8 hr	—	[66]

Table 2. Comparison of our process with previously reported ones.

Methods

To prepare SnO$_2$ nanostructures, Sn powder (1 g; Daejung Co., 99.9%) was placed in an alumina boat of a thermal evaporation furnace. The silicon substrate with 3-nm Au was placed upside down on the alumina boat to create conditions facilitating the adsorption of Au onto the substrate upon vaporisation. The temperature was raised to 900 °C at a rate of 10 °C/min, and an O$_2$-Ar mixture (97:3) was flown at a pressure of 2 Torr for 1 h at 900 °C.
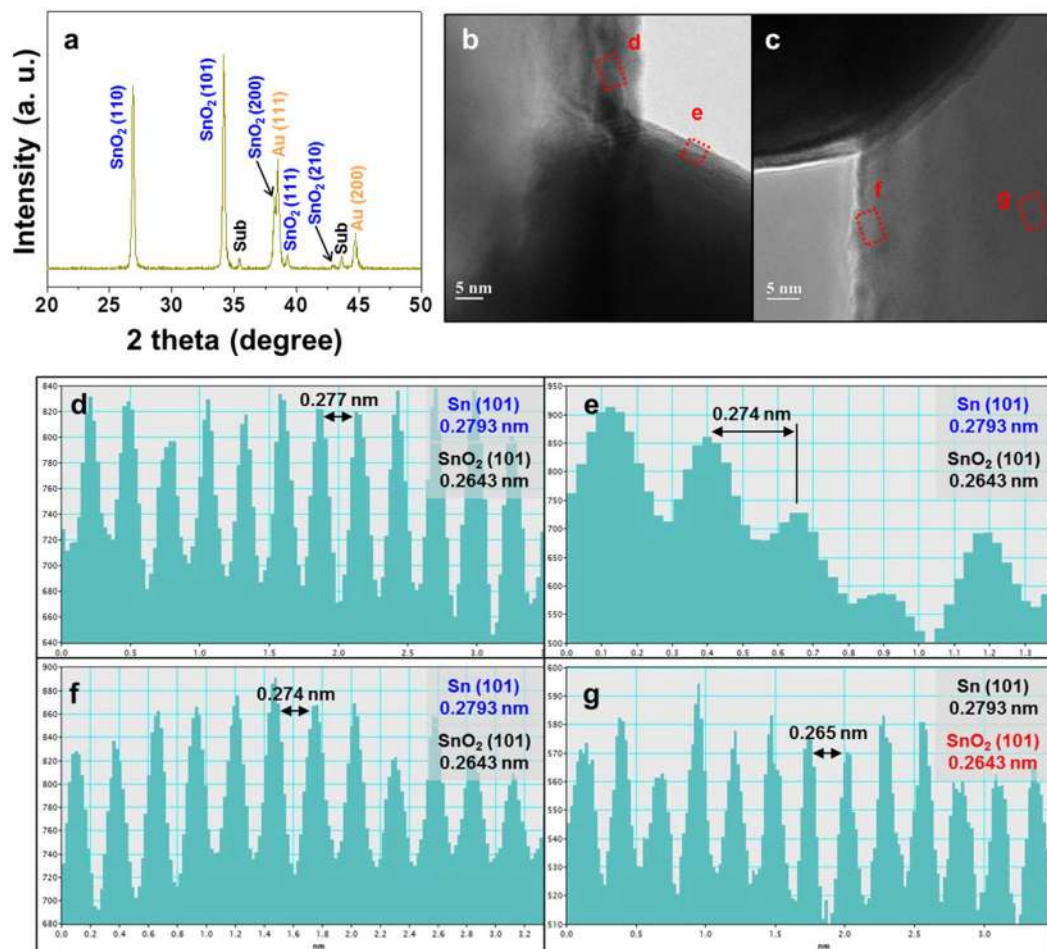
Figure 3. Crystallinity and microstructure of several parts of Au-decorated SnO_2 nanostructures. (**a**) XRD spectrum of Au-SnO_2 mixture; (**b,c**) HRTEM images acquired at the interface between a Au particle (dark region) and a SnO_2 nanowire (white region); (**d**) interplanar spacing showing the reduction of SnO_2 to Sn on the surface of SnO_2 nanowire; (**e**) interplanar spacing of SnO_2-based layers formed on the Au particle surface; (**f**) interplanar spacing confirming the reduction of SnO_2 to Sn, measured on the other surface of the SnO_2 nanowire; (**g**) interplanar spacing confirming the reduction of SnO_2 to Sn, measured inside the SnO_2 nanowire.

Gold Chloride hydrate 99.995% ($HAuCl_4 \cdot 4H_2O$ (0.23 g, 99.995%) and 2-propanol (10 g, 99.5%) were well mixed, and 3 mL of the mixture was dropped on the substrate part where the SnO_2 nanowires were to be synthesised. Thereafter, a flame with a temperature of 1300 °C was applied for 5 s in the standby state using a special flame chemical vapour deposition (FCVD) technique.

Morphology was probed by scanning electron microscopy (SEM; Hitachi S-4200, Hitachi) and transmission electron microscopy (TEM; JEM-2100F, JEOL), crystallinity was probed by X-ray diffraction (XRD; Philips X'pert diffractometer, Philips) and high-resolution transmission electron microscopy (HRTEM), while elemental composition was probed by XRD, elemental mapping, and energy-dispersive X-ray spectroscopy (EDX).

Data availability
All the data are available from the corresponding author on reasonable request.

References
1. Engel, T. & Reid, P. *Thermodynamics, statistical thermodynamics, and kinetics books a la carte edition (4rd Edition)*. (Pearson, 2018).
2. Hobson, A. *Physics: concepts and connections*. (Pearson, 2009).
3. Pahari, A. & Chauhan, B. *Engineering chemistry*. (Jones and Bartlett Publishers, 2007).
4. Rajkiewicz, M. *Chemical and Applied Engineering Materials: Interdisciplinary Research and Methodologies*. (CRC Press, 2015).
5. Shi, L., Liang, L., Ma, J. & Sun, J. Improved photocatalytic performance over AgBr/ZnO under visible light. *Superlattices Microstruct.* **62**, 128–139 (2013).
6. Ellis, B., Kan, W. H., Makahnouk, W. R. M. & Nazar, L. F. Synthesis of nanocrystals and morphology control of hydrothermally prepared $LiFePO_4$. *J. Mater. Chem.* **17**, 3248–3254 (2017).
7. Brown, A. J. *et al.* Interfacial microfluidic processing of metal-organic framework hollow fiber membranes. *Sci.* **345**, 72–75 (2014).

8. Jana, S., de Frutos, M., Davidson, P. & Abecassis, B. Ligand-induced twisting of nanoplatelets and their self-assembly into chiral ribbons. *Sci. Adv.* **3**, e1701483 (2017).

9. Nair, A. S. & Pathak, B. Computational Screening for ORR Activity of 3d Transition Metal Based M@Pt Core–Shell Clusters. *J. Phys. Chem. C.* **123**, 3634–3644 (2019).

10. Ramesh, S., Karuppasamy, K., Kim, H.-S., Kim, H. S. & Kim., J.-H. Hierarchical Flowerlike 3D nanostructure of Co$_3$O$_4$@MnO$_2$/N-doped Graphene oxide (NGO) hybrid composite for a high-performance supercapacitor. *Sci. Rep.* **8**, 16543 (2018).

11. Ji, J. *et al.* Guanidinium-based polymerizable surfactant as a multifunctional molecule for controlled synthesis of nanostructured materials with tunable morphologies. *ACS. Appl. Mater. Interfaces* **9**, 19124–19134 (2017).

12. Li, Y. & Huang, Y. Morphology-controlled synthesis of platinum nanocrystals with specific peptides. *Adv. Mater.* **22**, 221921–1925 (2010).

13. Sharifi, T. *et al.* Impurity-controlled crystal growth in low-dimensional bismuth telluride. *Chem. Mater.* **30**, 6108–6115 (2018).

14. Li, J. *et al.* Artificial compound eyes prepared by a combination of air-assisted deformation, modified laser swelling, and controlled crystal growth. *ACS Nano* **13**, 114–124 (2019).

15. Mao, Y. & Wong, S. S. Composition and shape control of crystalline Ca$_{1-x}$Sr$_x$TiO$_3$ perovskite nanoparticles. *Adv. Mater.* **172**, 194–2199 (2005).

16. Tongying, P. *et al.* Control of elemental distribution in the nanoscale solid-state reaction that produces (Ga$_{1-x}$Zn$_x$)(N$_{1-x}$O$_x$) nanocrystals. *ACS Nano* **11**, 8401–8412 (2017).

17. Shin, G. *et al.* SnO$_2$ nanowire logic devices on deformable nonplanar substrates. *ACS Nano* **5**, 10009–10016 (2011).

18. Choi, M. S. *et al.* Promotional effects of ZnO-branching and Au-functionalization on the surface of SnO$_2$ nanowires for NO$_2$ sensing. *J. Alloys Compd.* **786**, 27–39 (2019).

19. Yen, H., Seo, Y., Kaliaguine, S. & Kleitz, F. Role of metal–support interactions, particle size, and metal–metal synergy in CuNi nanocatalysts for H$_2$ generation. *ACS Catal.* **5**, 5505–5511 (2015).

20. Piotrowski, M. *et al.* Probing of thermal transport in 50 nm thick PbTe nanocrystal films by time-domain thermoreflectance. *J. Phys. Chem. C* **122**, 27127–27134 (2018).

21. Dong, J. *et al.* Facile synthesis of a nitrogen-doped graphene flower-like MnO$_2$ nanocomposite and its application in supercapacitors. *Appl. Surf. Sci.* **427**, 986–993 (2018).

22. Kim, J.-H., Mirzaei, A., Kim, H. W. & Kim, S. S. Extremely sensitive and selective sub-ppm CO detection by the synergistic effect of Au nanoparticles and core-shell nanowires. *Sens. Actuators B-Chem.* **248**, 177–188 (2017).

23. Wu, W. *et al.* Non-centrosymmetric Au–SnO$_2$ hybrid nanostructures with strong localization of plasmonic for enhanced photocatalysis application. *Nanoscale* **5**, 5628–5636 (2013).

24. Bing, Y. *et al.* Multistep assembly of Au-loaded SnO$_2$ hollow multilayered nanosheets for high-performance CO detection. *Sens. Actuators B-Chem.* **227**, 362–372 (2016).

25. Singh, N., Gupta, R. K. & Lee, P. S. Gold-nanoparticle-functionalized In$_2$O$_3$ nanowires as CO gas sensors with a significant enhancement in response. *ACS Appl. Mater. Interfaces* **3**, 2246–2252 (2011).

26. Steinhauer, S. *et al.* Thermal oxidation of size-selected Pd nanoparticles supported on CuO nanowires: the role of the CuO–Pd interface. *Chem. Mater.* **29**, 6153–6160 (2017).

27. Lai, X. *et al.* Ordered arrays of bead-chain-like In$_2$O$_3$ nanorods and their enhanced sensing performance for formaldehyde. *Chem. Mater.* **22**, 3033–3042 (2010).

28. Kwon, Y. J. *et al.* Enhancement of the benzene-sensing performance of Si nanowires through the incorporation of TeO$_2$ heterointerfaces and Pd-sensitization. *Sens. Actuators B-Chem.* **239**, 1085–1097 (2017).

29. Kim, J.-H., Mirzaei, A., Kim, H. W. & Kim, S. S. Combination of Pd loading and electron beam irradiation for superior hydrogen sensing of electrospun ZnO nanofibers. *Sens. Actuators B-Chem.* **284**, 628–637 (2019).

30. Pargar, F., Kolev, H., Koleva, D. A. & van Breugel, K. Microstructure, surface chemistry and electrochemical response of Ag|AgCl sensors in alkaline media. *J. Mater. Sci.* **53**, 7527–7550 (2018).

31. Mehrer, H. *Diffusion in solids.* (Springer, 2007).

32. Lee, J. W. *et al.* Morphological modulation of urchin-like Zn$_2$SnO$_4$/SnO$_2$ hollow spheres and their applications as photocatalysts and quartz crystal microbalance measurements. *Appl. Surf. Sci.* **474**, 78–84 (2019).

33. Zuo, S. *et al.* SnO$_2$/graphene oxide composite material with high rate performance applied in lithium storage capacity. *Electrochim. Acta* **264**, 61–68 (2018).

34. Liu, Q., Xu, Y., Qiu, X., Huang, C. & Liu, M. Chemoselective hydrogenation of nitrobenzenes activated with tuned Au/h-BN. *J. Catal.* **370**, 55–60 (2019).

35. Plodinec, M. *et al.* Black TiO$_2$ nanotube arrays decorated with Ag nanoparticles for enhanced visible-light photocatalytic oxidation of salicylic acid. *J. Alloys Compd.* **776**, 883–896 (2019).

36. Kim, N.-H. *et al.* Highly sensitive and selective acetone sensing performance of WO$_3$ nanofibers functionalized by Rh$_2$O$_3$ nanoparticles. *Sens. Actuator B-Chem.* **224**, 185–192 (2016).

37. Woo, H.-S., Na, C. W., Kim, I.-D. & Lee, J.-H. Highly sensitive and selective trimethylamine sensor using one-dimensional ZnO–Cr$_2$O$_3$ hetero-nanostructures. *Nanotechnology* **23**, 245501 (2012).

38. Chen, X. H. & Moskovits, M. Observing catalysis through the agency of the participating electrons: Surface-chemistry-induced current changes in a tin oxide nanowire decorated with silver. *Nano Lett.* **7**, 807–812 (2007).

39. Lee, S. *et al.* Effects of annealing temperature on the H$_2$-sensing properties of Pd-decorated WO$_3$ nanorods. *Appl. Phys. A-Mater. Sci. Process.* **124**, 232 (2018).

40. Kwak, C.-H., Woo, H.-S. & Lee, J.-H. Selective trimethylamine sensors using Cr$_2$O$_3$-decorated SnO$_2$ nanowires. *Sens. Actuators B-Chem.* **204**, 231–238 (2014).

41. Huang, S.-H. *et al.* Structures and catalytic properties of PtRu electrocatalysts prepared via the reduced RuO$_2$ nanorods array. *Langmuir* **24**, 2785–2791 (2008).

42. Sun, G.-J. *et al.* Synthesis of TiO$_2$ nanorods decorated with NiO nanoparticles and their acetone sensing properties. *Ceram. Int.* **42**, 1063–1069 (2016).

43. Rodríguez-Aguado, E. *et al.* Au nanoparticles supported on nanorod-like TiO$_2$ as catalysts in the CO-PROX reaction under dark and light irradiation: Effect of acidic and alkaline synthesis conditions. *Int. J. Hydrogen Energy* **44**, 923–936 (2019).

44. Gan, X., Li, X., Gao, X., Zhuge, F. & Yu, W. ZnO nanowire/TiO$_2$ nanoparticle photoanodes prepared by the ultrasonic irradiation assisted dip-coating method. *Thin Solid Films* **518**, 4809–4812 (2010).

45. Kukkola, J. *et al.* Room temperature hydrogen sensors based on metal decorated WO$_3$ nanowires. *Sens. Actuators B-Chem.* **186**, 90–95 (2013).

46. Lee, J.-S., Katoch, A., Kim, J.-H. & Kim, S. S. Effect of Au nanoparticle size on the gas-sensing performance of p-CuO nanowires. *Sens. Actuators B-Chem.* **222**, 307–314 (2016).

47. Trung, D. D. *et al.* Effective decoration of Pd nanoparticles on the surface of SnO$_2$ nanowires for enhancement of CO gas -sensing performance. *J. Hazard. Mater.* **265**, 124–132 (2014).

48. Formo, E., Lee, E., Campbell, D. & Xia, Y. Functionalization of electrospun TiO$_2$ nanofibers with Pt nanoparticles and nanowires for catalytic applicaiton. *Nano Lett.* **8**, 668–672 (2008).

49. Chang, S.-J., Hsueh, T.-J., Chen, I.-C. & Huang, B. R. Highly sensitive ZnO nanowire CO sensors with the adsorption of Au nanoparticles. *Nanotechnology* **19**, 175502 (2008).

50. Chen, X. *et al.* NO$_2$ sensing properties of one-pot-synthesized ZnO nanowires with Pd functionalization. *Sens. Actuators B-Chem.* **280**, 151–161 (2019).

51. Dong, W. *et al.* Room-temperature solution synthesis of Ag nanoparticles functionalized molybdenum oxide nanowires and their catalytic applications. *Nanotechnology* **23**, 425602 (2012).

52. Jang, B.-H. *et al.* Selectivity enhancement of SnO$_2$ nanofiber gas sensors by functionalization with Pt nanocatalysts and manipulation of the operation temperature. *Sens. Actuators B-Chem.* **188**, 156–168 (2013).

53. Chen, X. *et al.* Synthesis of ZnO nanowires/Au nanoparticles hybrid by a facile one-pot method and their enhanced NO$_2$ sensing properties. *J. Alloy. Compd.* **783**, 503–512 (2019).

54. Chávez, F. *et al.* Sensing performance of palladium-functionalized WO$_3$ nanowires by a drop-casting method. *Appl. Surf. Sci.* **275**, 28–35 (2013).

55. Shin, J., Choi, S.-J., Youn, D.-Y. & Kim, I.-D. Exhaled VOCs sensing properties of WO$_3$ nanofibers functionalized by Pt and IrO$_2$ nanoparticles for diagnosis of diabetes and halitosis. *J. Electroceram.* **29**, 106–116 (2012).

56. Choi, S.-W., Katoch, A., Kim, J.-H. & Kim, S. S. Prominent reducing gas-sensing performances of n-SnO$_2$ nanowires by local creation of p−n heterojunctions by functionalization with p-Cr$_2$O$_3$ nanoparticles. *ACS Appl. Mater. Interfaces* **6**, 17723–17729 (2014).

57. Tak, Y., Hong, S. J., Lee, J. S. & Yong, K. Solution-based synthesis of a CdS nanoparticle/ZnO nanowire heterostructure array. *Cryst. Growth Des.* **9**, 2627–2632 (2009).

58. Yin, H., Yu, K., Song, C., Huang, R. & Zhu, Z. Synthesis of Au-decorated V$_2$O$_5$@ZnO heteronanostructures and enhanced plasmonic photocatalytic activity. *ACS Appl. Mater. Interfaces* **6**, 14851–14860 (2014).

59. Chen, T., Xing, G. Z., Zhang, Z., Chen, H. Y. & Wu, T. Tailoring the photoluminescence of ZnO nanowires using Au nanoparticles. *Nanotechnology* **19**, 435711 (2008).

60. Shin, J. *et al.* Thin-wall assembled SnO$_2$ fibers functionalized by catalytic Pt nanoparticles and their superior exhaled-breath-sensing properties for the diagnosis of diabetes. *Adv. Funct. Mater.* **23**, 2357–2367 (2013).

61. Li, L., Gu, L., Lou, Z., Fan, Z. & Shen, G. ZnO quantum dot decorated Zn$_2$SnO$_4$ nanowire heterojunction photodetectors with drastic performance enhancement and flexible ultraviolet image sensors. *ACS Nano* **11**, 4067–4076 (2017).

62. Aluri, G. G. *et al.* Highly selective GaN-nanowire/TiO$_2$-nanocluster hybrid sensors for detection of benzene and related environment pollutants. *Nanotechnology* **22**, 295503 (2011).

63. Lu, M.-L., Lin, T.-Y., Weng, T.-M. & Chen, Y.-F. Large enhancement of photocurrent gain based on the composite of a single n-type SnO$_2$ nanowire and p-type NiO nanoparticles. *Opt. Express* **19**, 16772 (2011).

64. Pan, J. *et al.* SnO$_2$@CdS nanowire-quantum dots heterostructures: tailoring optical properties of SnO$_2$ for enhanced photodetection and photocatalysis. *Nanoscale* **5**, 3022–3029 (2013).

65. Park, S. *et al.* Light-activated NO$_2$ gas sensing of the networked CuO-decorated ZnS nanowire gas sensor. *Appl. Phys. A* **122**, 504 (2016).

66. Peng, C., Wang, W., Zhang, W., Liang, Y. & Zhuo, L. Surface plasmon-driven photoelectrochemical water splitting of TiO$_2$ nanowires decorated with Ag nanoparticles under visible light illuminaiton. *Appl. Surf. Sci.* **420**, 286–295 (2017).

Acknowledgements

Author contributions

M.S.C., H.G.N. and S.K. developed the concept and H.W.K. and C.J. wrote the manuscript. M.S.C., H.G.N., J.H.B. and W.S.O. fabricated the samples and performed the measurements. S.-W.C., S.S.K. and K.H.L. provided theoretical basis. All authors contributed to interpretation of the fundamental theories, discussed the issues, and exchanged views on the manuscript.

Competing interests

The authors declare no competing interests.

Additional information

Supplementary information is available for this paper at https://doi.org/10.1038/s41598-019-57222-z.

Correspondence and requests for materials should be addressed to H.W.K. or C.J.

Reprints and permissions information is available at www.nature.com/reprints.

Publisher's note Springer Nature remains neutral with regard to jurisdictional claims in published maps and institutional affiliations.